HiSST: International Conference on
High-Speed Vehicle Science Technology

26–29 November 2018, Moscow, Russia

Two-Equation Transition Model Based on Intermittency and Empirical Correlations

Jeroen Van den Eynde[1] *& Johan Steelant*[2]

Abstract

A two-equation correlation-based transition model is presented to predict the onset and development of the laminar-turbulent transition process for boundary layers. It uses one equation for the intermittency-transport, and another for the transport of a transition onset criterion. It uses some elements from the Langtry-Menter intermittency-based γ-$Re_{\theta t}$ transition model, but introduces a physics-based rationale for the intermittency production and destruction. The model has been validated for a number of subsonic to hypersonic boundary layer cases and is able to correctly predict the transition onset location and typical skin friction overshoot.

Keywords: *transition, modelling, intermittency, empirical*

Nomenclature

Latin

$\mathcal{C}$ – Model constant
C_f – Skin friction coefficient
C_p – Pressure coefficient
c – Velocity
$\mathcal{D}$ – Diffusion term
$\mathcal{E}$ – Dissipation term
k – Turbulent kinetic energy
K – Pressure gradient parmeter
M – Mach number
n – Spatial coordinate normal to streamline
$\mathcal{P}$ – Production term
Pr – Prandtl number
PRC – Pressure relaxation factor
p – Pressure
q – Dynamic pressure
$\dot{q}$ – heat flux
$Re_{\theta t}$ – Transition momentum Reynolds number
r – Recovery factor
S_{ij} – Strain rate tensor
St – Stanton number
s – Spatial coordinate along streamline
T – Temperature
Tu – Turbulence level
u, U – Velocity
v – Wall-normal velocity
x – Spatial coordinate

Greek

α – Onset parameter
β – Turbulent spot growth
δ – Boundary layer thickness
γ – Intermittency
μ – Dynamic viscosity
ν – Kinematic viscosity
$\hat{n}\sigma$ – Spot growth parameter
θ – Momentum thickness
τ – Shear stress
ρ – Density

Superscripts

$'$ – Fluctuating value
$\bar{}$ – Favre-averaged

Subscripts

i, j – Components of vector
∞ – Freestream value
ad – Adiabatic
c – Critical value; Compressible
e – Edge value
inc – Incompressible
l – Laminar value
t – Turbulent value; Value at transition onset
r – Recovery
w – Value at the wall

[1]*Research Fellow, ESA/ESTEC, 2200AG Noordwijk, The Netherlands (Jeroen.Van.den.Eynde@esa.int)*
[2]*Senior Aerothermodynamicist, ESA/ESTEC, 2200AG Noordwijk, The Netherlands (Johan.Steelant@esa.int)*

1. Introduction

The laminar-turbulent transition process is still difficult to accurately predict in many engineering applications. It is however of great importance, as it can affect the resulting aerodynamic, structural and aero-thermal loads. Even though some of the mechanisms that govern transition are well understood, a single complete model that can predict the transition processes in a Reynolds-Averaged Navier-Stokes (RANS) context, for a wide range of flow regimes, has not yet been found.

The easiest way of computing "transition" from the laminar to the turbulent flow regime is to simply enable the turbulence model at a predefined onset location. This method completely ignores the mechanisms behind the transition process, and thus both the length and position of the transitional region have been found to be incorrect when applied to the current turbulence models [1, 2]. A more mechanism-based approach is therefore needed to accurately predict all the characteristics of laminar-turbulent transition. The concept of intermittency, essentially a blending parameter between the laminar and turbulent state of a boundary layer, can be used to have a more physical representation of the transitional flow. A transport equation for intermittency γ was developed by Steelant & Dick [3–6] that aims to reproduce the γ-distribution function in the transition region, proposed by Dhawan & Narasimha [7]. The original work of Steelant & Dick used two sets of conditionally-averaged Navier-Stokes equations, effectively doubling the computational effort and storage requirement. This limitation was removed by Suzen & Huang [8] who implemented a γ-transport equation, based on the models of Steelant & Dick and Cho & Chung [9], into a single set of RANS equations. An important factor in the development of a RANS model is that it is dependent only on local variables, such that it can easily be implemented in unstructured CFD solvers without the need for integral values or line-searching algorithms. A local correlation-based transition model was presented by Menter et al [10] and Langtry et al [11]. This model is built on the SST $k-\omega$ turbulence model and uses two additional transport equations for the intermittency γ and transition onset momentum thickness Reynolds number $Re_{\theta t}$. This model, referred to as the Langtry-Menter γ-$Re_{\theta t}$ transition model, has gained quite some traction in the transition modelling community. Several authors have built upon this model, to extend it to hypersonic flows [12, 13] and transition induced by crossflow instability [14, 15].

Recently a new laminar-turbulent transition model was presented, $\gamma-\alpha$, that is only dependent on local flow variables [16], similar to the γ-$Re_{\theta t}$ model. It uses a more physics-based γ-transport equation, and is completely based on empirical correlations describing the envisaged flow nature. Instead of a transport equation for the transition momentum-thickness Reynolds number $\tilde{Re}_{\theta t}$, an alternative parameter is constructed that allows the transition onset to be evaluated at the wall. The transition model does not alter the turbulent kinetic energy equation, such that it is fully decoupled from the turbulence model. The current work presents a slightly revised version of the $\gamma-\alpha$ model [16] and gives a more detailed description of some of the model terms.

2. Model Formulation

The proposed model has been developed originally with the aim of improving the γ-$Re_{\theta t}$ model by replacing the intermittency transport equation with a more physical model based on turbulent spot growth. In addition, experimentally derived correlations are incorporated to account for compressibility, wall temperature effects, etc. Contrary to the original γ-$Re_{\theta t}$ model, the evaluation of transition onset is performed at the wall instead of inside the boundary layer. For this reason the $\tilde{Re}_{\theta t}$-transport equation is replaced by a transport equation of an alternative parameter α, that allows for the onset to be evaluated at the wall. Only locally computed flow variables are used such that it can easily be implemented in unstructured CFD solvers without the need for algorithms to determine integral flow quantities. The transition model is also fully decoupled from any turbulence model, i.e. no modification of the turbulent kinetic energy equation is needed, and hence it can be principally combined with any preferred turbulence model. Although an earlier version of the $\gamma-\alpha$ model was presented by Van den Eynde et al [16], the complete description is given here for completeness.

2.1. Reynolds stress closure term

The interface between the proposed transition model and the turbulence model is purely based on the definition of an *effective* eddy viscosity μ_t^*, such that the transition model is fully decoupled from the

used turbulence model and the latter is interchangeable.

Following the conditioned Navier-Stokes concept of Steelant & Dick [3], the Reynolds stress can be worked out as

$$\overline{u_i' u_j'} = (\gamma - 1)\left(\overline{u_i' u_j'}\right)_l + \gamma\left(\overline{u_i' u_j'}\right)_t \tag{1a}$$

$$= (\gamma - 1)\,\overline{u_{i,l}' u_{j,l}'} + \gamma\,\overline{u_{i,t}' u_{j,t}'} + \gamma(\gamma - 1)\,\left(\overline{u_i}_l - \overline{u_i}_t\right)\left(\overline{u_j}_l - \overline{u_j}_t\right) \tag{1b}$$

where subscripts $()_l$ and $()_t$ are respectively the laminar and turbulent contributions. The first and second terms are the laminar and turbulent Reynolds stress, while the third term in (1b) is due to the velocity profile change between the laminar and turbulent phase, and can be seen as the passing of a large turbulent eddy. By assuming that this large eddy contribution can be represented as $\overline{u_{i,t}' u_{j,t}'}$ and the laminar Reynolds stress neglected, the overall Reynolds stress can be approximated by

$$\overline{u_i' u_j'} \approx \gamma\,\overline{u_{i,t}' u_{j,t}'} + \gamma\,(1 - \gamma)\,\overline{u_{i,t}' u_{j,t}'} \tag{2a}$$

$$= [\gamma + \gamma\,(1 - \gamma)]\,\overline{u_{i,t}' u_{j,t}'} \tag{2b}$$

where $-\rho\,\overline{u_{i,t}' u_{j,t}'} = 2\,\mu_t\,S_{ij}$ with strain-rate tensor S_{ij}.

Preliminary evaluation and boundary layer measurements by Blair [17] indicated that the large eddy contribution may account for about 15% of the shear stress. This contribution has therefore been enhanced and modified empirically to yield the overshoot of skin friction and heat transfer coefficient, typically observed during the transition process. The resulting Reynolds stress closure term of the current model becomes then

$$-\rho\,\overline{u_i' u_j'} = 2\,\mu_t^* S_{ij} \tag{3}$$

where the effective eddy viscosity μ_t^* is given by

$$\mu_t^* = \left[\gamma + \gamma\,(1 - \gamma)\,\mathcal{C}_{\mu_{t_1}}\left(1 + \tanh\left(\frac{\gamma - \mathcal{C}_{\mu_{t_2}}}{\mathcal{C}_{\mu_{t_3}}}\right)\right)\right]\mu_t \tag{4}$$

with model constants

$$\mathcal{C}_{\mu_{t_1}} = 0.5, \quad \mathcal{C}_{\mu_{t_2}} = 0.25, \quad \mathcal{C}_{\mu_{t_3}} = 0.1\,.$$

A similar derivation can be performed for the energy equation resulting in an identical closure for the transitional heat fluxes, i.e.

$$-\rho\,\overline{u_i' T'} = \frac{\mu_t^*}{Pr_t}\frac{\partial T}{\partial x_i} \quad . \tag{5}$$

With respect to the normal stresses, the same approach is followed such that

$$k_t^* = [\gamma + \gamma\,(1 - \gamma)]\,k_t \quad . \tag{6}$$

These normal stresses are contributing to an effective pressure $p^* = p + \frac{2}{3}\rho k^*$, to be added in both the momentum equation and the energy equation.

2.2. Intermittency transport equation

The intermittency transport equation used in the current model is given by

$$\frac{\partial\,(\rho\,\gamma)}{\partial t} + \frac{\partial\,(\rho\,U_j\,\gamma)}{\partial x_j} = \mathcal{P}_\gamma - \mathcal{E}_\gamma + \mathcal{D}_\gamma \tag{7}$$

in which $\mathcal{P}_\gamma$, $\mathcal{E}_\gamma$ and $\mathcal{D}_\gamma$ are respectively the production, dissipation and diffusion terms of the intermittency γ. These individual terms are based on the original terms developed by Steelant & Dick [3–6], and were constructed based on analytical derivations and experimentally derived engineering correlations. For the sake of completeness, all terms are presented in detail in the current work, even when the original formulations [3–6] are used.

2.2.1. Production of γ

The production term $\mathcal{P}_\gamma$ is based on the concept of turbulent spot growth and is computed by

$$\mathcal{P}_\gamma = 2\, f_\gamma\, (1-\gamma)\, \sqrt{-\ln(1-\gamma)}\, \beta\, \overline{\rho}\, \tilde{c}\,. \tag{8}$$

In this equation, the term f_γ is a damping function that gradually ramps up the production during the initial stages of transition to mimic the distributed breakdown mechanism, and is defined as [4]

$$f_\gamma = \begin{cases} 1 - \exp\left[-\mathcal{C}_{f_{\gamma_1}} \tan\left(\mathcal{C}_{f_{\gamma_2}}\gamma - \mathcal{C}_{f_{\gamma_3}}\right) - \mathcal{C}_{f_{\gamma_4}}\right] & \text{for } \gamma < 0.45 \\ 1 & \text{for } \gamma \geq 0.45 \end{cases} \tag{9}$$

with model constants

$$\mathcal{C}_{f_{\gamma_1}} = 1.735, \quad \mathcal{C}_{f_{\gamma_2}} = 5.45, \quad \mathcal{C}_{f_{\gamma_3}} = 0.95375, \quad \mathcal{C}_{f_{\gamma_4}} = 2.2\,.$$

The variables $\overline{\rho}$ and $\tilde{c}$ in (8) are respectively the Reynolds-averaged density and Favre-averaged flow velocity magnitude. The term β accounts for the turbulent spot growth and is given by

$$\beta = \sqrt{\hat{n}\sigma(K, Tu)}\, \frac{\overline{c}_\infty \rho_\infty}{\mu_\infty} \tag{10}$$

with the spot growth parameter defined as

$$\hat{n}\sigma = 1.25 \times 10^{-11}\, Tu_\infty^{7/4}\, f_K\, f_{\mathsf{M},\hat{n}\sigma}\, f_{T_w,\hat{n}\sigma}\,. \tag{11}$$

As a pressure gradient has an effect on the spot growth, the spot growth parameter is modified using the same correlation as in Steelant & Dick [3]:

$$f_K = 1 + f_\gamma(PRC - 1) \tag{12}$$

where f_γ is the distributed breakdown parameter given in (9) and the pressure relaxation factor PRC is given by

$$PRC = \begin{cases} \left(474 Tu_\infty^{-2.9}\right)^{\left(1-\exp\left(2\times 10^6\, K\right)\right)} & \text{for } K < 0 \\ 10^{-3227\, K^{0.5985}} & \text{for } K \geq 0 \end{cases}. \tag{13}$$

The pressure gradient parameter K is defined for compressible flows as

$$K = -\frac{\mu_\infty}{\rho_\infty^2 U_\infty^3} \left|1 - M_\infty^2\right| \frac{dp}{ds} \tag{14}$$

where M is the local Mach number and $\frac{dp}{ds}$ is the derivative of pressure p along the streamline direction s.

The compressibility correction $f_{\mathsf{M},\hat{n}\sigma}$ in (11) is defined by [5]

$$f_{\mathsf{M},\hat{n}\sigma} = \left(1 + 0.58\, M_\infty^{0.6}\right)^{-2}\,. \tag{15}$$

The term $f_{T_w,\hat{n}\sigma}$ in (11) is a correction to account for the wall temperature effect on the turbulent spot growth. It needs to be further defined.

2.2.2. Dissipation of γ

The γ-dissipation term $\mathcal{E}_\gamma$ has been constructed such that the wall-normal variation of the intermittency goes to zero near the wall. It has been found that the product of normal derivatives of the velocity amplitude and the intermittency automatically satisfies this property [4]. Therefore the $\mathcal{E}_\gamma$-term is chosen to be proportional to this product. In addition the term should be dimensionally consistent with viscosity, which yields

$$\mathcal{E}_\gamma = \mathcal{C}_{\mathcal{E}_\gamma}\, \mu_\gamma\, \frac{\tilde{c}}{\tilde{c}_\infty^2} \frac{\partial \tilde{c}}{\partial n} \frac{\partial \gamma}{\partial n}\,. \tag{16}$$

The intermittency-viscosity μ_γ is constructed to approximately reproduce the inverse Klebanoff function describing the wall-normal distribution of intermittency inside the boundary layer. This intermittency-viscosity was originally derived by Steelant & Dick [4] to be expressed as

$$\mu_\gamma = \frac{v}{v_\infty}\frac{v_\infty}{n\,u_\infty}\frac{\rho\,u_\infty\delta_\omega}{\mu}\frac{\gamma}{1-\gamma}\left[-\ln(1-\gamma)\right]^{-\frac{n-1}{n}}\mu \tag{17}$$

where the constant n was later defined to be equal to 6. In the original derivation, the term $\frac{\gamma}{1-\gamma}$ was removed to avoid the singularity for $\gamma \to 1$. The term $\frac{v}{v_\infty}$ was replaced by a near-wall damping function to bring μ_γ to zero near the wall. The term $\frac{\rho\,u_\infty\delta_\omega}{\mu}$, which is equivalent to a Reynolds number, was replaced in [4] by a term proportional to a correlation for the critical momentum thickness Reynolds number, dependent on the freestream turbulence level, whereas $\frac{v_\infty}{u_\infty}$ was treated as a constant.

However, by considering a Blasius profile for the boundary layer, it could be derived that

$$\frac{v_\infty}{u_\infty} \sim \frac{1}{\sqrt{Re_x}}\ . \tag{18}$$

By following the rationale Steelant & Dick [4] and assuming the Reynolds number-like term $\frac{\rho\,u_\infty\delta_\omega}{\mu}$ is proportional to the momentum thickness Reynolds number, it can be assumed that

$$\frac{\rho\,u_\infty\delta_\omega}{\mu} \sim Re_\theta \approx 0.664\sqrt{Re_x}\ . \tag{19}$$

Therefore, by combining (18) and (19), the premultiplication factor in (17) cancels out. Equation (17) can then be rewritten as

$$\mu_\gamma = \mathcal{C}_{\mu_{\gamma_1}}\left[-\ln(1-\gamma)\right]^{-\frac{5}{6}(1-\gamma)}\mu\,f_{\mu_\gamma}\,f_{\mathsf{M},\mu_\gamma} \tag{20}$$

with a near-wall damping function

$$f_{\mu_\gamma} = 1 - \exp\left[-\mathcal{C}_{\mu_{\gamma_2}}\left(\frac{y\,\bar{c}_\infty}{\nu_\infty}\right)^2\right] \tag{21}$$

constructed to set the γ-viscosity coefficient to zero near the wall. This formulation in (20) is an update to the earlier $\gamma-\alpha$ model presented in [16] in which the original formulation of [4] was still used.

The compressibility correction factor $f_{\mathsf{M},\mu_\gamma}$ is constructed to capture the effect of an overall thicker boundary layer at high Mach numbers and the downstream movement of the transition onset at higher Mach numbers. For the latter, a compressibility correction derived by Narasimha [18] is used, who stated that the transition onset Reynolds number increases like

$$\frac{Re_{x_c}}{Re_{x_{inc}}} = \left[1 + 0.38\,M_e^{0.6}\right]\ . \tag{22}$$

Based on boundary layer thickness, using the relation $\delta/x = 5/\sqrt{Re_x}$ for a Blasius boundary layer, this can then be written as:

$$\frac{\delta_c}{\delta_{inc}} = \sqrt{1 + 0.38\,M_e^{0.6}}\ . \tag{23}$$

For the former, a compressibility correction for the boundary layer thickness [19] has been simplified to be independent of the temperature distribution in the boundary layer. The ratio of compressible to incompressible boundary layer displacement thickness is given in [19] as

$$\frac{\delta_c}{\delta_{inc}} = \sqrt{C_w}\left[1 + \left[0.2 + 0.9\frac{T_w}{T_{ad}}\right]\frac{\gamma-1}{5}M_e^2\right] \tag{24}$$

where the Chapman-Rubesin correction can be approximated as:

$$C_w \approx \left(\frac{T^*}{T_e}\right)^{-\frac{1}{3}} = \left[0.46 + 0.54\frac{T_w}{T_e} + 0.16\,r\,\frac{\gamma-1}{2}M_e^2\right]^{-\frac{1}{3}}\ .$$

In the case of an adiabatic plate, $T_w = T_{ad}$, the above ratio reduces to

$$\frac{\delta_c}{\delta_{inc}} = \sqrt{C_w}\left[1 + 0.22\,(\gamma-1)\,M_e^2\right] \tag{25}$$

with $C_w = \left[1 + 0.7\,r\,\frac{\gamma-1}{2}M_e^2\right]^{-\frac{1}{3}}$. The overall thickening effect is simplified as

$$\frac{\delta_c}{\delta_{inc}} = 1 + \mathcal{C}\frac{\gamma-1}{2}M_e^2\,. \tag{26}$$

The resulting overall compressibility correction factor in (20) is then given by the combination of the shift of transition onset (23) and the boundary layer thickening (26):

$$f_{\mathsf{M},\mu_\gamma} = \left[1 + \mathcal{C}_{\mu_{\gamma_3}}\frac{\gamma-1}{2}M_\infty^2\right]\sqrt{1 + 0.38\,M_\infty^{0.6}}\,. \tag{27}$$

The model constants in these equations are defined as:

$$\mathcal{C}_{\mathcal{E}_\gamma} = 20.0, \quad \mathcal{C}_{\mu_{\gamma_1}} = 0.57, \quad \mathcal{C}_{\mu_{\gamma_2}} = 256.0, \quad \mathcal{C}_{\mu_{\gamma_3}} = 0.26\,.$$

2.2.3. Diffusion of γ

The γ-diffusion term $\mathcal{D}_\gamma$ is simply defined as

$$\mathcal{D}_\gamma = \frac{\partial}{\partial x_i}\left[\mu_\gamma\frac{\partial\gamma}{\partial x_i}\right]. \tag{28}$$

Note that in the original γ-$Re_{\theta t}$ model the diffusion coefficient was given by a combination of the molecular viscosity and eddy viscosity, whereas in the current model the γ-viscosity, as defined is (20), is used.

2.3. Transition onset

The original γ-$Re_{\theta t}$ model used a transport equation to transport the transition momentum thickness Reynolds number $Re_{\theta t}$, computed outside the boundary layer, towards the wall, essentially giving access to a freestream value within the boundary layer. The transition onset point is then evaluated within the boundary layer by comparing the transported $Re_{\theta t}$ with the strain rate Reynolds number defined as $Re_v = \frac{\rho y^2 S}{\mu}$, which is a local variable.

The current model regulates the transition onset by setting $\mathcal{P}_\gamma = 0$ and $\gamma = 0.01$ at the wall whenever transition should not occur. Away from the wall, the γ-production term is unchanged. Essentially, the production term in (8) is pre-multiplied by an onset switch $F_{\mathsf{onset}} \in \{0, 1\}$. Because the onset is evaluated at the wall, where the strain rate Reynolds number is zero, an evaluation criterion different from the original γ-$Re_{\theta t}$ model needs to be defined.

2.3.1. Evaluation of transition onset

Following the Thwaites-Waltz methodology [19], the momentum thickness for an incompressible boundary layer can be derived from the shear stress at the wall and the shear correlation function $S(\Lambda)$, i.e.

$$\tau_w = \frac{\mu\,U_\infty}{\theta}\,S(\Lambda) \tag{29}$$

or in terms of the momentum-thickness Reynolds number:

$$\tau_w = \frac{2\,q_\infty\,S(\Lambda)}{Re_\theta}\,. \tag{30}$$

Using the Chapman-Rubesin correction, this can be extended towards compressible boundary layers as

$$\tau_w = \frac{2\,q_\infty\,S(\Lambda)}{Re_\theta}\sqrt{\frac{\rho_w\,\mu_w}{\rho_\infty\,\mu_\infty}}\,. \tag{31}$$

In these equations the shear correlation factor $S(\Lambda)$ is approximated as [19]

$$S = (0.09 + \Lambda)^{0.62} \tag{32}$$

and the pressure gradient parameter Λ can be computed using

$$\Lambda = \left(\theta^2/\nu\right) \frac{dU_\infty}{ds} = -Re_\theta^2 \frac{\mu}{\rho U_\infty^3} \frac{dp}{ds} . \tag{33}$$

Equation (31) can be rearranged to obtain

$$\frac{2\, q_\infty\, S(\Lambda)}{Re_\theta} \frac{1}{\sqrt{\rho_\infty \mu_\infty}} = \tau_w \frac{1}{\sqrt{\rho_w \mu_w}} \tag{34}$$

By grouping the freestream variables and the wall variables, as in (34), the former can be computed in the freestream outside the boundary layer and transported, while the latter can be computed at the wall to evaluate the transition onset. These groups are respectively defined as

$$\alpha \coloneqq \frac{2\, q_\infty\, S(\Lambda)}{Re_\theta} \frac{1}{\sqrt{\rho_\infty \mu_\infty}} \tag{35a}$$

$$\tau_w^* \coloneqq \tau_w \frac{1}{\sqrt{\rho_w \mu_w}} . \tag{35b}$$

These two terms are of great importance in the current model, since they define the transition onset. In the γ-$Re_{\theta t}$ model of Langtry-Menter [20] transition onset occurs when the boundary layer momentum thickness Reynolds number becomes larger than a critical onset momentum thickness Reynolds number $Re_{\theta t}$. Equivalently, following the definition in (35), it can be said transition onset occurs when the local wall value τ_w^* becomes lower than a critical $\alpha_c = \alpha_c(Re_{\theta t})$.

Therefore, the transition onset switch F_{onset} is

$$F_{\text{onset}} = \begin{cases} 1 & \text{if} \quad \tau_w^* \leq \alpha_c \qquad (36a) \\ 0 & \text{otherwise} \ . \qquad (36b) \end{cases}$$

After the transition onset, the shear stress at the wall — and thus also τ_w^* — will increase towards a turbulent value above α_c, which would set F_{onset} back to zero if no additional criterion is defined. To avoid this behaviour, F_{onset} is kept to one whenever transition is occurring, i.e. when $\gamma \geq 0.01 + \epsilon$. An additional criterion to allow for relaminarisation will be implemented in the future.

2.3.2. Transport equation for α

Instead of using a transport equation for $Re_{\theta t}$, the current model uses a transport equation for α

$$\frac{\partial\left(\rho\,\alpha\right)}{\partial t} + \frac{\partial\left(\rho\, U_j\, \alpha\right)}{\partial x_j} = \mathcal{P}_\alpha - \mathcal{N}_\alpha + \mathcal{D}_\alpha \tag{37}$$

whose production and diffusion terms are the same as those in the original γ-$Re_{\theta t}$ model, except for the transported scalar and some model constants. The goal of this approach is to transport the critical α_c value, computed using the transition momentum thickness Reynolds number $Re_{\theta t}$ in the freestream, towards the wall where it can be compared to the value of τ_w^*.

The production term of α is defined as

$$\mathcal{P}_\alpha = \mathcal{C}_{\mathcal{P}_{\alpha 1}} \frac{\rho}{t} \left(\alpha_c - \alpha\right) \left(1 - F_{\mathcal{P}_\alpha}\right) \tag{38}$$

with time scale $t = 500\mu/\rho U^2$ and blending function

$$F_{\mathcal{P}_\alpha} = \min\left[\max\left[F_{\text{wake}} \exp\left(-(y/\delta)^4\right); 1.0 - \left(\frac{\gamma - 1/\mathcal{C}_{\mathcal{P}_{\alpha 2}}}{1 - 1/\mathcal{C}_{\mathcal{P}_{\alpha 2}}}\right)^2\right]; 1.0\right] . \tag{39}$$

The other terms in $F_{\mathcal{P}_\alpha}$, i.e. δ and F_{wake}, follow the definition of the original γ-$Re_{\theta t}$ model:

$$\delta = 375\,\frac{Re_{\theta t}\,\mu}{\rho\,U}\,\frac{\Omega\,y}{U}; \qquad F_{\text{wake}} = e^{-\left(\frac{Re_\omega}{10^5}\right)^2}; \qquad Re_\omega = \frac{\rho\,\omega\,y^2}{\mu}\,. \tag{40}$$

The diffusion term of α is defined as

$$\mathcal{D}_\alpha = \frac{\partial}{\partial x_i}\left[\mathcal{C}_{\mathcal{D}_\alpha}\,(\mu+\mu_t)\,\frac{\partial \alpha}{\partial x_i}\right]. \tag{41}$$

As in the case of the original γ-$Re_{\theta t}$ model, a significant lag occurs between the freestream value and the transported value at the wall. This is not in accordance with experiments when freestream values are acting nearly locally onto the boundary layer. Diffusion is clearly not the only driving transport mechanism of freestream perturbations to the wall, but predominantly driven by the local pressure coupling. This results into a wall-normal evolution of α, which is modelled here simply by a term that drives the wall-normal gradient of α to zero:

$$\mathcal{N}_\alpha = \mathcal{C}_{\mathcal{N}_\alpha}\,\rho\,|\overline{c}|\,\frac{\partial \alpha}{\partial n}\,. \tag{42}$$

In these equations, the model constants are defined as:

$$\mathcal{C}_{\mathcal{P}_{\alpha 1}} = 0.3, \quad \mathcal{C}_{\mathcal{P}_{\alpha 2}} = 50, \quad \mathcal{C}_{\mathcal{N}_\alpha} = 0.4, \quad \mathcal{C}_{\mathcal{D}_\alpha} = 2.0\,.$$

2.3.3. Transition onset criterion

The critical value of the transition momentum thickness Reynolds number $Re_{\theta t}$ used in the definition of α is obtained using experimentally derived correlations. Many correlations exist, e.g. Abu-Ghannam and Shaw [21], but in this work a correlation similar to that proposed by Steelant & Dick [4] is used:

$$Re_{x,c} = 400094\,Tu_\infty^{-1.38} - 105254\,Tu_\infty^{-7/8}\,. \tag{43}$$

Note that in the original Steelant & Dick model, which is based on the correlation by Mayle [22], i.e. $Re_{\theta t} = 420.0\,Tu_{le,\infty}^{-0.69}$, but introduces the effect of distributed breakdown, the freestream turbulence level is taken at the leading edge. By applying the assumption of a Blasius profile, this can be written in function of the momentum thickness Reynolds number. Additionally a compressibility correction is added to yield the transition onset correlation

$$Re_{\theta c} = 0.664\,\sqrt{400094\,Tu_\infty^{-1.38} - 105254\,Tu_\infty^{-7/8}}\;f_{\mathsf{M},Re_{\theta c}} \tag{44}$$

with

$$f_{\mathsf{M},Re_{\theta c}} = \sqrt{1 + 0.38\,M_\infty^{0.6}}\,. \tag{45}$$

2.4. Additional remarks

2.4.1. Computation of freestream values

The proposed model relies on knowing the *local* freestream values of turbulence level, velocity and Mach number, density and viscosity, which are required near the wall for the computation of the γ-production and γ-dissipation. The turbulence level Tu_∞ can be computed using the local value of the transported α since its value should be the same as the freestream α-value. From α one can deduce the computed critical momentum thickness Reynolds number, after which the transition onset correlation can be iteratively solved to find the corresponding turbulence level. The freestream velocity, density and Mach number can be computed by assuming isentropic conditions and using the isentropic flow relations. Although this is not strictly valid, especially with the presence of shocks, it is currently being used as a first-order approximation without many issues, because the transition occurs before the occurrence of shocks in the current cases.

Table 1. Experimental set-up of the validation cases.

Case	U_∞ $[m/s]$	ρ_∞ $[kg/m^3]$	$Re_{\infty,1}$ $[m^{-1}]$	$Tu_{\infty,le}$ [%]	μ_t/μ_l [-]	$Tu_{\infty,le}$ [%]	μ_t/μ_l [-]
T3A	5.4	1.2	3.60×10^5	3.3	14.0	2.8	8.0
T3B	9.4	1.2	6.27×10^5	6.2	100.0	5.1	60.0
T3A-	19.8	1.2	1.32×10^6	1.0	7.5	0.8	5.0
T3C5	8.4	1.2	5.60×10^5	2.7	15.0	2.2	10.0
				isotropic		anisotropic	

Case	M_∞ [-]	p_0 [bar]	T_0 $[K]$	T_w $[K]$	$Re_{\infty,1}$ $[m^{-1}]$	$Tu_{\infty,le}$ [%]	μ_t/μ_l [-]	$Tu_{\infty,le}$ [%]	μ_t/μ_l [-]
RWG-M6[a]	5.98	12.94	548.8	297.0	9.44×10^6	0.7*	200.0	0.6	200.0
RWG-M6-SBLI[b]	5.98	13.15	511.4	297.0	10.77×10^6	0.7*	200.0	0.6	200.0
						isotropic		anisotropic	

[a] This case is the RWG1 experiment at $Re_1 = 9.35 \times 10^6\, m^{-1}$ presented in Sandham et al. (2014) [28].
[b] This case is the RWG2 experiment at $Re_1 = 10.66 \times 10^6\, m^{-1}$ presented in Sandham et al. (2014) [28].
* Estimated from the pressure fluctuations measured in the RWG facility at similar flow conditions. [29]

2.4.2. Stability of the model

The coupling of the transition model to the turbulence model makes the system of equations more complex. To ensure the stability of the discretised problem, the source terms of the additional transition model equations need to be treated with a relaxation method that restricts the time-step. More information about this method can be found in the work of Steelant & Dick [23, 24] and Merci et al [25].

3. Validation

The current transition model was implemented in the unstructured CFD solver DLR-TAU, developed by the Deutsches Zentrum für Luft- und Raumfahrt (DLR), and was validated for flat-plate boundary layers, both in subsonic and hypersonic conditions. Menter's SST $k-\omega$ model [26] was used as underlying turbulence model for the current simulations. Unstructured grids were used with prismatic layers near the walls (with first cell heights always set to have $y^+ < 1$) to capture the boundary layers and tetrahedral elements away from the walls. Adaptive grid refinement was applied to properly resolve shocks and contact discontinuities.

The validation cases consist of some of the classical ERCOFTAC T3-series experiments in the incompressible regime [27] and Mach 6 flat-plate experiments (with and without shock-wave boundary-layer interaction) performed under contract of the European Space Agency (ESA) [28–30]. The experimental results obtained in the DNW Ludwieg tube in Göttingen [28, 29] are used for the current comparison. An overview of the flow parameters of the different cases can be found in Table 1.

In order to get simulation results that are as representative as possible to the wind tunnel experiments, the inlet conditions were carefully selected. An effort has been made in particular to match the turbulence level and turbulence decay in the freestream above the flat plate, since the transition behaviour is highly dependent on it.

An important note has to be made regarding the measurement of turbulent fluctuations and the definition

of the turbulent kinetic energy. Formally the turbulence level is defined as

$$Tu = \sqrt{\frac{2}{3}\frac{k}{U_\infty^2}} \tag{46}$$

with the turbulent kinetic energy k given as

$$k = \frac{1}{2}\left(u'^2 + v'^2 + w'^2\right) . \tag{47}$$

When assuming isotropic turbulence, this can be expressed using a single velocity fluctuation component:

$$k_{\text{iso}} = \frac{3}{2}u'^2 \qquad \text{or} \qquad Tu_{\text{iso}} = \frac{u'}{U_\infty} \tag{48}$$

while for anisotropic it can be assumed that the streamwise fluctuations are of the same magnitude as the other components combined, i.e.

$$k_{\text{aniso}} = \frac{1}{2}\left(u'^2 + \underbrace{v'^2 + w'^2}_{\approx u'^2}\right) \approx u'^2 \qquad \text{or} \qquad Tu_{\text{aniso}} = \sqrt{\frac{2}{3}}\frac{u'}{U_\infty} . \tag{49}$$

This means that, depending on the assumption, the defined turbulence levels can vary more than 20% for a single value of the streamwise fluctuating component. In addition, there can be a significant uncertainty on the measurement of the turbulent fluctuations, including a dependence on the measurement methodology. For example, for the T3-series experiments both single-wire and cross-wire anemometry measurements are available, but the turbulence levels that would be computed using these two methods can vary considerably[3].

The turbulence level in high-speed wind tunnels is difficult to measure and often not reported in literature. For the current RWG-M6 cases, the total pressure RMS levels were measured and reported [29]. Following the assumptions of hypersonic and low turbulence intensity conditions, and assuming Morkovin's hypothesis holds true, the streamwise turbulent fluctuation (and therefore the turbulence level) can be estimated by [31, 32]:

$$\frac{u'}{U_\infty} = \frac{2\,p_0'}{C_p\,\overline{\rho}\,U_\infty^2\,[2 + (\gamma - 1)\,M_t^2]} \tag{50}$$

where p_0' is the total pressure fluctuation level, C_p is the pressure coefficient downstream of a normal shock and M_t is the turbulent Mach number. The resulting turbulence level estimate for the current hypersonic cases is reported in Table 1. It should be noted that this methodology is to be used with care because of the strong assumptions (e.g. neglecting acoustic fluctuations).

The uncertainties in the freestream turbulence levels can thus have a large effect on the resulting transition computations and the comparison with experiments. In order to quantify the effect of this uncertainty, two sets of simulations were run with different freestream turbulence conditions for each test case. The first set assumes the isotropic definition of (48) and uses the turbulence levels as presented in Table 1 *(isotropic columns)*, corresponding to the single-wire measurements in the case of

[3]For the T3A experiment, the single-wire u'-fluctuation measurement in the freestream furthest downstream (1450 mm from the leading edge) is given as 1.10%. A single-wire measurement can actually not distinguish the streamwise (u') and wall-normal (v') fluctuation components and thus measures both. The cross-wire u', v' and w' measurements at the same location are given as respectively 1.00%, 0.93% and 0.91%. A difference of 16% is therefore observed between the turbulence levels resulting from the single-wire and cross-wire measurements of the T3A experiment at this position. Closer to the leading edge, where the level of anisotropy is higher, the difference becomes 23%. Summarising thsee results for cases T3A, T3A-, T3B and T3C5, the discrepancies are in the range of 16-23%, 12-13%, 11-18% and 1-4% respectively. No cross-wire measurements were available near the leading edge for case T3A-, so that its discrepancy range might be ever larger.

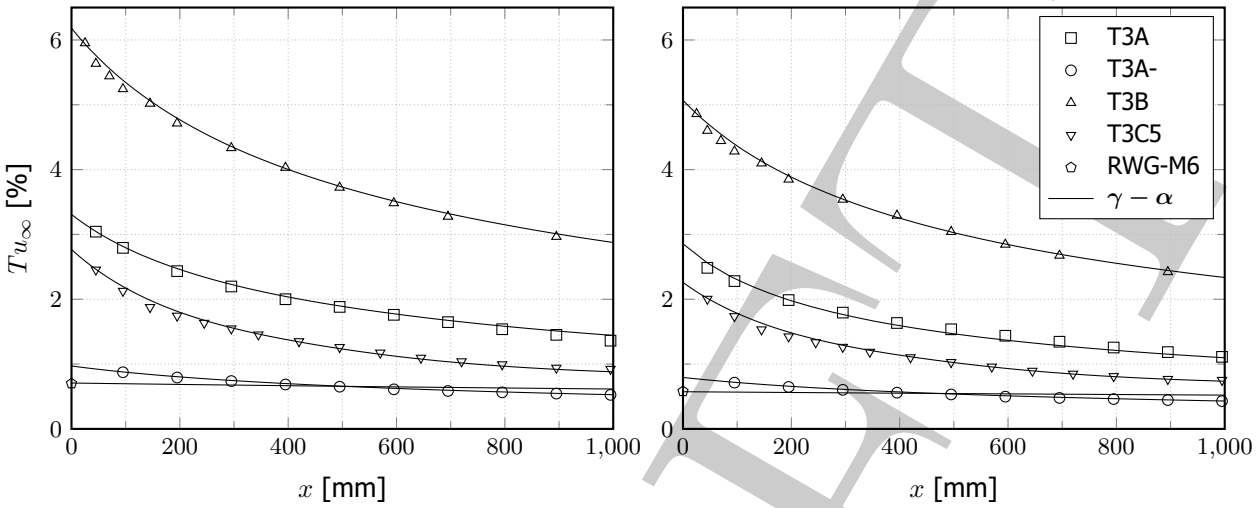

Fig 1. Freestream turbulence levels of the different cases for the isotropic *(left)* and anisotropic *(right)* set of results.

the T3 experiments. The second set assumes the anisotropic definition of (49) and uses the same measurements rescaled with a factor $\sqrt{2/3} \approx 82\%$. The two sets of results will thus define an uncertainty region in which the model predicts the experimental results to be. The first and second set, hereafter called isotropic and anisotropic respectively, will respectively be plotted using —— and ——, while the resulting uncertainty region will be shaded as ▒ in subsequent figures that include both sets.

The computed freestream turbulence for all the validation cases in this work and the corresponding experimental target values are given in Figure 1 *(left)* and *(right)* for the isotropic and anisotropic set respectively. It shows that the turbulence levels match very well with the experimental data points of the ERCOFTAC T3-series [27] along the length of the flat plate. Since only a single estimate of the turbulence level for the hypersonic RWG-M6 cases is available, this value is kept nearly constant throughout the domain by prescribing a large value of μ_t/μ_l, as shown in Table 1.

3.1. ERCOFTAC Series: T3A(-), T3B and T3C5

Four cases from the ERCOFTAC T3-series have been simulated to include a large range of freestream turbulence levels (T3A, T3A- and T3B) and a pressure gradient (T3C5) in the validation study. All cases were computed with the current γ-α model using the two sets of inflow conditions as described before, and the original Langtry-Menter γ-$Re_{\theta t}$ model [20, 33] (as implemented in DLR-TAU) using the isotropic set of conditions.

3.1.1. T3A

The skin friction coefficient for the T3A case is given in Figure 2, which shows the experimental measurements, the simulations using the two transition models and the theoretical laminar and turbulent values according to the Blasius and Schultz-Grunow relations.

From this figure it can be seen that the experimental data points are in the middle of the uncertainty region, i.e. the two γ-α results are on either side of the experimental data points. The computed skin friction peaks are approximately $\Delta Re_x \approx 50\,000$ and $100\,000$ before and after the measurements for respectively the isotropic and anisotropic results. It clearly indicates the sensitivity of the transition behaviour to the exact freestream turbulence level and thus highlights the need for accurate experimental measurements and descriptions. The steepness of the skin friction rise matches well with the experimental observations and also the typical skin friction overshoot is captured by the γ-$Re_{\theta t}$ model.

The γ-$Re_{\theta t}$ model matches the initial transition onset behaviour almost exactly, but under-predicts the skin friction near the end of the transition process. The good agreement between the γ-$Re_{\theta t}$ model and the T3A experimental transition onset is not surprising, since it was used as validation case during

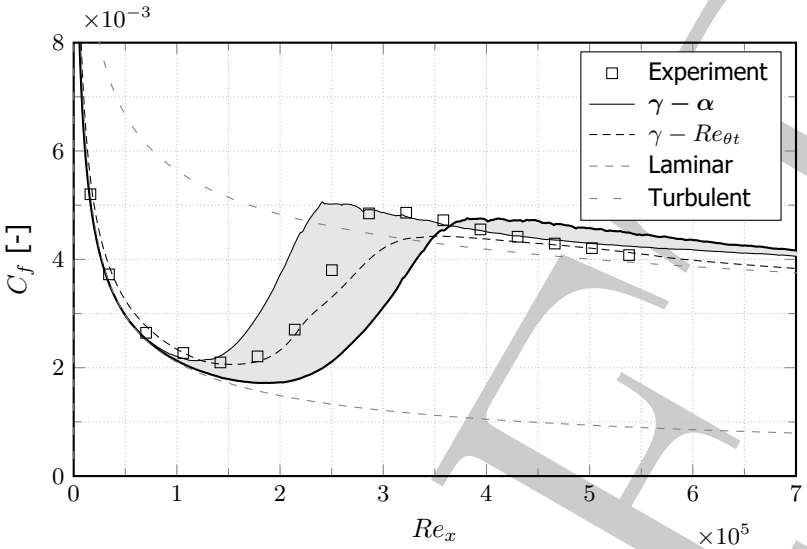

Fig 2. Skin friction coefficient for the T3A flat plate boundary layer case.

the development of the model [33]. It should be noted that the turbulence level used for the γ-$Re_{\theta t}$ simulation is the published isotropic value, which is actually 16-23% higher than the anisotropic cross-wire measurements as mentioned before[3]. If the measured anisotropic freestream turbulence levels would be used, the agreement would not hold. This justifies the rationale behind the two sets conditions and resulting uncertainty region used in this work.

3.1.2. T3A-

The T3A- test case is similar to the previous experiment but uses a much lower turbulence level ($< 1\%$). Due to this low turbulence level the transition onset will be far downstream, making it very sensitive to the flow conditions.

This sensitivity can be seen in the large uncertainty region between the isotropic and anisotropic γ-α results, shown in Figure 3. This figure shows that all simulations — including the γ-$Re_{\theta t}$ model — seem to predict transition upstream of the actual location determined experimentally. *It should be noted that, at the time of writing, the anisotropic result is not yet fully converged. This is the reason why fully turbulent values are not reached after the transition onset. A fully turbulent skin friction is expected to be reached after complete convergence.*

The steepness of the skin friction increase at the beginning of the transition process is correctly resolved by both the γ-α and γ-$Re_{\theta t}$ model, although the latter seems to over-predict the skin friction coefficient before the onset.

3.1.3. T3B

The T3B test case has a high turbulence level ($5 - 6\%$), which will trigger transition onset near the flat plate leading edge.

Figure 4 shows the skin friction coefficient results for the T3B case. It clearly shows that the isotropic and anisotropic results of the γ-α model match well with the experimental data points, both in transition onset location as in the steepness of the skin friction rise. The isotropic results seem to transition slightly before the experimental measurements, while the anisotropic results lie slightly after. However, the difference is very small. It was expected that the anisotropic results would match better, since it was found that the cross-wire measurements were approximately 18% lower than the isotropic value[3] near the leading edge and thus close to the freestream turbulence levels of the anisotropic set.

The results computed using the γ-$Re_{\theta t}$ model do not match well with the experimental measurements. The skin friction is over-predicted before and initially during the transition process, while the peak

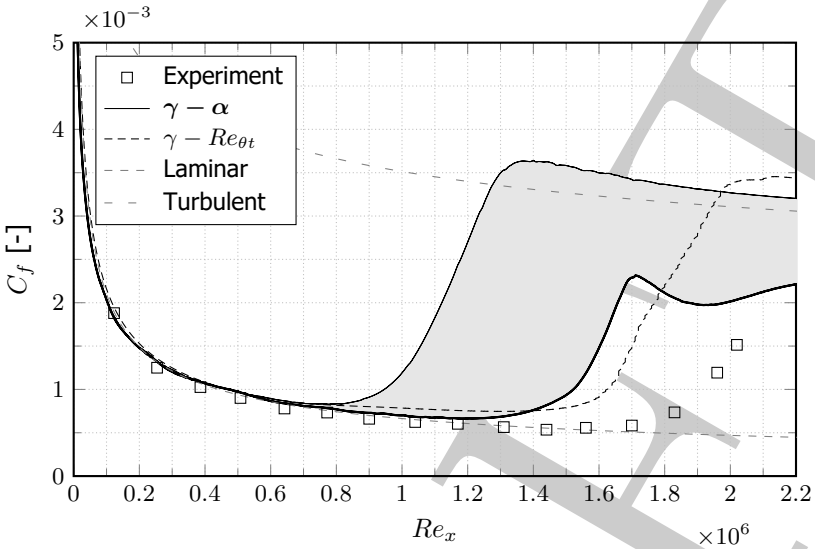

Fig 3. Skin friction coefficient for the T3A- flat plate boundary layer case.

skin friction coefficient is under-predicted. Also the steepness of the skin friction rise is highly under-predicted.

3.1.4. T3C5

So far the test cases were zero-pressure-gradient flat plate experiments at various turbulence levels. The T3C5 case in the T3-series includes the effect of a pressure gradient (both favourable and adverse). The first 0.9 m of the flat plate (approx. up to $Re_x \approx 5.0 \times 10^5$) is under a favourable pressure gradient, while an adverse pressure gradient is applied thereafter.

In the simulations, this pressure gradient is achieved by a suitably shaped Euler wall opposite the flat plate. The resulting wall pressure profile along the domain is given in Figure 5, and is compared to the experimental measurements. It can be seen that a good agreement is reached between the simulations and the wind tunnel measurements.

Figure 6 shows the skin friction coefficient results for the T3C5 case. The isotropic results are closer to the experiments than the anisotropic results for the transition onset location, which is as expected since the cross-wire measurements showed that the level of anisotropy was only 1-4%[3]. The anisotropic results, which have a lower freestream turbulence level, predict the transition onset after the experimentally measured onset. In both cases the skin friction rise is too steep and the γ-α model consistently over-predicts the skin friction coefficient during and after the transition process. *It should be noted that these results are not fully converged yet, and are expected to slightly improve.*

3.2. RWG-M6 Series

Two hypersonic flat-plate experiments at Mach 6, with and without shock-wave boundary-layer interaction, were computed numerically. A comparison is made here between the numerical results of the γ-α model, the γ-$Re_{\theta t}$ model and the experimental measurements [28–30].

Because the original γ-$Re_{\theta t}$ model was not developed for high-speed flows, it has been extended by Krause et al [12, 13] to hypersonic flows by introducing updated correlations. This version of the γ-$Re_{\theta t}$ model is also available in DLR-TAU and is also used in the current comparisons. In addition, the DLR-TAU code includes a limiter on the turbulent kinetic energy production term, based on the damping effect caused by shock unsteadiness [34], in order to avoid spurious values of the turbulent kinetic energy after a shock. This limiter has been enabled for all the simulations of the RWG-M6 series.

The value of the wall temperature correction factor $f_{T_w,\hat{n}\sigma}$ in (11) will be of importance to the correct transition behaviour of the Mach 6 cases. A full definition of this factor has not yet been suggested in this

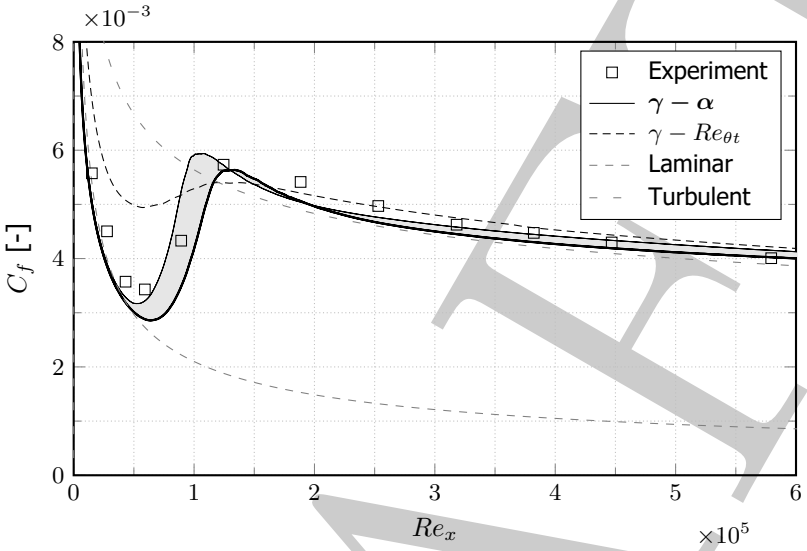

Fig 4. Skin friction coefficient for the T3B flat plate boundary layer case.

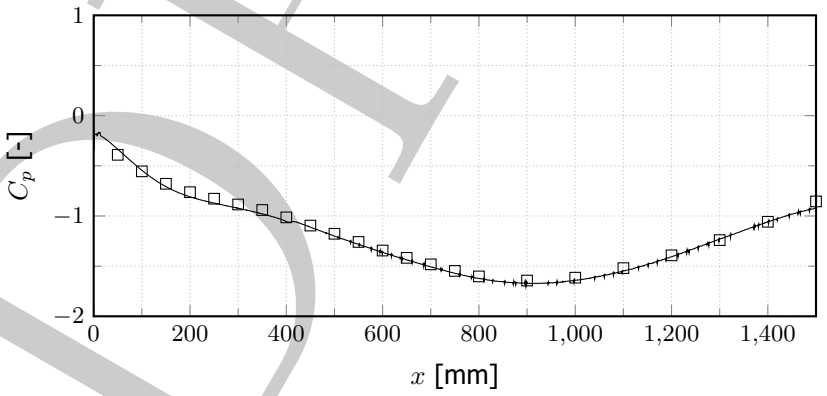

Fig 5. Pressure coefficient on the wall for the T3C5 flat plate boundary layer case.

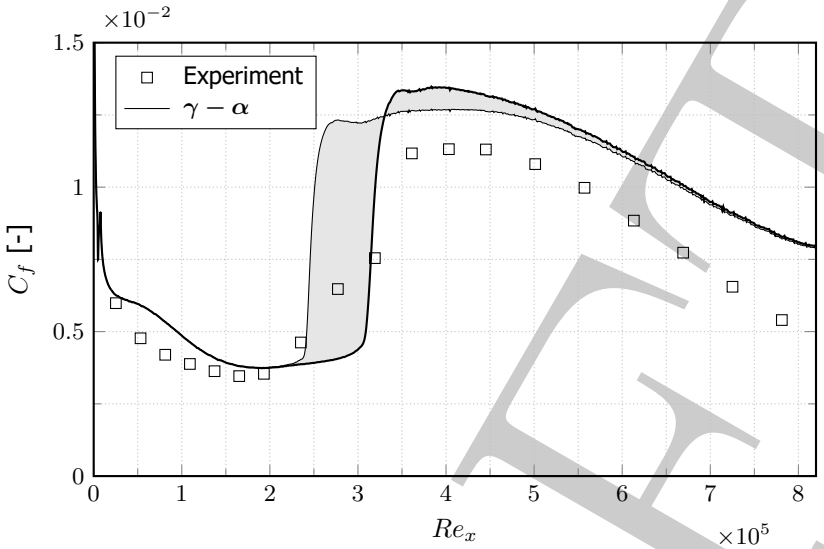

Fig 6. Skin friction coefficient for the T3C5 flat plate boundary layer case.

work. However, based on the studies of the wall temperature effect on turbulent spot growth [35–37], the turbulent spot spreading angle was estimated to be 50% lower for the current Mach 6 cooled-wall cases, with $T_w/T_0 = 0.5 - 0.6$, than for corresponding hot-wall cases. Hence the value of the wall temperature correction factor is set to $f_{T_w,\hat{n}\sigma} = 0.25$ in the γ-α model for the simulations. However, a further investigation into the wall temperature effect is required to properly define this correction factor and its dependencies. A first effort to deduce empirical correlations for compressibility and temperature effects can be found in [38].

3.2.1. RWG-M6

The RWG-M6 case, which is a Mach 6 flat-plate boundary layer without impinging shock, is simulated using the γ-α , standard γ-$Re_{\theta t}$ and hypersonic γ-$Re_{\theta t}$ [12, 13] models. The computed Stanton number for all simulations, here defined using the recovery temperature T_r as

$$St = \frac{\dot{q}_w}{\rho_\infty U_\infty c_p \left(T_r - T_w\right)} \tag{51}$$

to match the definition used in the published experimental results, is given in Figure 7.

From this figure, it is immediately evident that both the standard γ-$Re_{\theta t}$ model and the hypersonic extension by Krause cannot correctly predict the transition behaviour and resulting heat transfer. While the hypersonic γ-$Re_{\theta t}$ model seems to approach the correct onset location, the Stanton number is highly under-predicted throughout the transition and the peak heating is not captured.

In contrast, the proposed γ-α model captures the steepness and the typical overshoot of the heat flux increase very well, and the peak Stanton number is only off by roughly 5%. The location of the transition onset, and subsequently the location of the peak heating, is however predicted too far downstream for both the isotropic and anisotropic results. *Currently model improvements are being performed to improve the transition onset prediction for hypersonic boundary layers.* In any case, the performance of the γ-α model is remarkably more accurate than both the standard γ-$Re_{\theta t}$ model and the γ-$Re_{\theta t}$ model with the hypersonic extension by Krause, both qualitatively and quantitatively.

3.2.2. RWG-M6-SBLI

The RWG-M6-SBLI case has very similar flow conditions as the RWG-M6 case (as can be seen in Table 1), but includes an oblique shock impinging the boundary layer near the end of the transition process. Both in the experimental and numerical set-up this is achieved by using a shock generator placed opposite

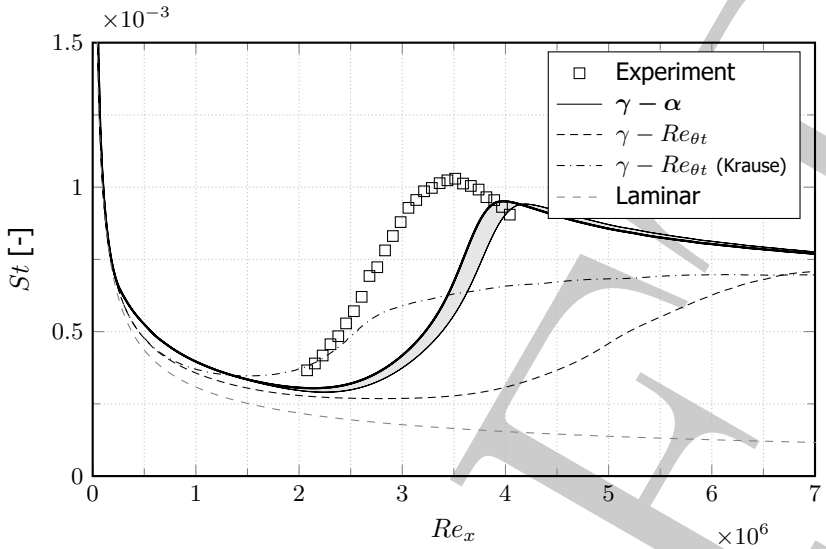

Fig 7. Stanton number for the RWG-M6 hypersonic boundary layer case.

the flat plate [28]. Also this case is simulated using the γ-α , standard γ-$Re_{\theta t}$ and hypersonic γ-$Re_{\theta t}$ models and compared to the experimental measurements.

The results are shown in Figure 8 and clearly indicate the poor agreement of the standard γ-$Re_{\theta t}$ model with the experiments. Because it does not capture the transition, as was already seen in case RWG-M6, the boundary layer is still laminar when the shock impinges. This results in a large shock-induced separation region and strongly under-predicted heat flux on the whole plate. The peak Stanton number is under-predicted with a factor of 3 approximately. The γ-$Re_{\theta t}$ model with Krause's hypersonic extension also does not capture the transition behaviour adequately, as was already shown in Figure 7. However, since the boundary layer is already transitional at the impingement point, the resulting heat flux after the shock is much higher than for the standard model and matches the experimental measurements reasonably well. Because the transition is not accurately captured, a turbulent boundary layer is not yet developed sufficiently, i.e. the boundary layer is too thin, and the location of the peak heating is predicted slightly downstream.

The transition behaviour is predicted much better by the γ-α model. In this case, the isotropic results predict transition onset too soon, while the anisotropic results match the experimental measurements very well. The location of the peak heat flux is in good agreement, but the actual peak Stanton number is under-predicted for the isotropic results because the boundary layer is already fully turbulent at the impingement point. The peak Stanton number for the anisotropic results is in good agreement with the experiments. These results indicate that the proposed γ-α model is capable of accurately simulating transition of hypersonic boundary layers, both without and with shock-wave boundary-layer interaction.

4. Conclusion

A new correlation-based laminar-turbulent transition model is proposed to predict the bypass transition process for subsonic to hypersonic boundary layers. It uses elements from the original intermittency-based γ-$Re_{\theta t}$ transition model but introduces a physics-based rationale for the production and destruction of intermittency, completely based on empirical correlations. It is fully decoupled from the underlying turbulence model, such that it can be used with any turbulence model considered most suitable for the envisaged application. Instead of a transport equation for the transition momentum-thickness Reynolds number $\tilde{Re}_{\theta t}$, such as in the γ-$Re_{\theta t}$ model, it introduces the transported parameter α that allows the evaluation of certain freestream flow variables at the wall and which controls the transition onset.

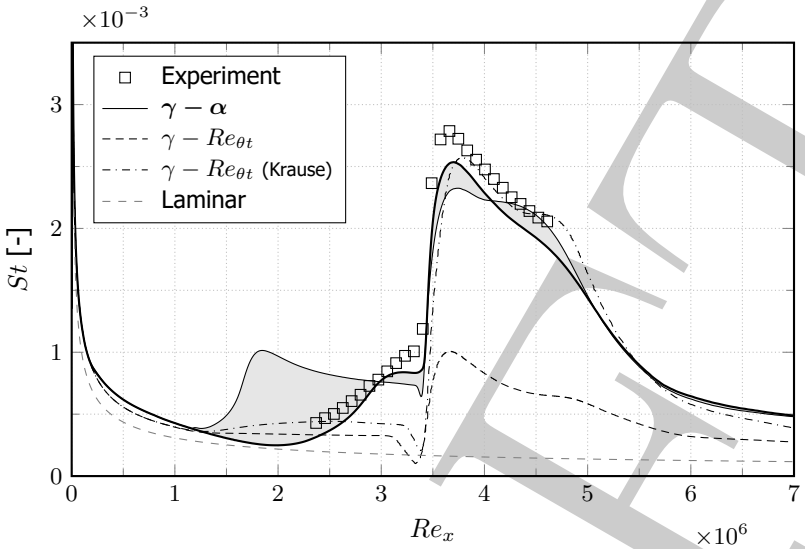

Fig 8. Stanton number for the RWG-M6-SBLI hypersonic shock-wave boundary-layer interaction case.

The proposed γ-α model has been tested using a variety of validation cases. The validation cases consist of the T3A, T3A-, T3B and T3C5 cases from the classical ERCOFTAC T3-series experiments in the incompressible regime, and Mach 6 flat-plate experiments (with and without shock-wave boundary-layer interaction) performed in the DNW Ludwieg tube in Göttingen. It has been shown that the γ-α model can accurately predict the transition process qualitatively (i.e. the steepness of skin friction and Stanton number increase during transition) for all zero-pressure gradient cases, both subsonic and hypersonic. Also the effect of a Mach 6 shock impingement is correctly captured and the peak heating is in good agreement with the experiments. This qualitative transition behaviour has been found to not always be adequately resolved by the γ-$Re_{\theta t}$ model, especially not for the hypersonic cases. The steepness of the skin friction rise for the non-zero pressure gradient does not completely match with the experiments, which will need to be investigated further.

Because laminar-turbulent transition is very sensitive to the actual flow conditions, accurate experimental measurements are of crucial importance for the correct numerical reconstruction and thus robust transition modelling. The current validation cases were performed with two sets of freestream turbulence conditions, different by about 20%, yielding two sets of results that define an uncertainty region. The produced simulation results showed that this uncertainty region can be quite large, especially for cases with low freestream turbulence levels. For most cases, the experimental measurements fall within this region computed using the γ-α model. It has been observed that the current model performs better than the γ-$Re_{\theta t}$ model in predicting the transition onset location if the actual turbulence levels — measured using for example cross-wire anemometry — would be imposed.

Although certain elements of the current model need to be further defined or fine-tuned, the current work shows the strong potential of the formulation. The model can accurately predict the qualitative transition behaviour for both subsonic and hypersonic transition to turbulence, including shock-wave boundary-layer interaction. It has been found to perform better than the γ-$Re_{\theta t}$ model for the Mach 6 cases, even when a modified γ-$Re_{\theta t}$ model is used, specifically tailored to hypersonic flows.

Acknowledgements

This work was made possible thanks to the Post-Doctoral Research Fellowship of the European Space Agency granted to the first author. The authors would like to thank Dr. Andrea Passaro, Dr. Luca Ferracina and Dan Fries for contributions to the development and implementation of the model, and Dr. Volker Hannemann for supporting implementation aspects into DLR-TAU.

References

[1] Savill, A. M., "Evaluating Turbulence Model Predictions of Transition," *Advances in Turbulence IV*, Springer Netherlands, 1993, pp. 555–562. doi:10.1007/978-94-011-1689-3_86.

[2] Westin, K. J. A., and Henkes, R. A. W. M., "Application of Turbulence Models to Bypass Transition," *Journal of Fluids Engineering*, Vol. 119, No. 4, 1997, p. 859. doi:10.1115/1.2819509.

[3] Steelant, J., and Dick, E., "Modelling of Bypass Transition with Conditioned Navier-Stokes Equations Coupled to an Intermittency Transport Equation," *International Journal for Numerical Methods in Fluids*, Vol. 23, 1996, pp. 193–220.

[4] Steelant, J., and Dick, E., "Prediction of by-pass transition by means of a turbulence weighting factor - Part I : Theory and Validation," *ASME paper 99-GT-29*, 1999.

[5] Steelant, J., and Dick, E., "Prediction of By-Pass Transition by Means of a Turbulence Weighting Factor: Part II — Application on Turbine Cascades," *ASME paper 99-GT-30*, ASME, 1999. doi: 10.1115/99-GT-030.

[6] Steelant, J., and Dick, E., "Modeling of Laminar-Turbulent Transition for High Freestream Turbulence," *Journal of Fluids Engineering*, Vol. 123, No. 1, 2001, p. 22. doi:10.1115/1.1340623.

[7] Dhawan, S., and Narasimha, R., "Some properties of boundary layer flow during the transition from laminar to turbulent motion," *Journal of Fluid Mechanics*, Vol. 3, No. 04, 1958, p. 418. doi: 10.1017/S0022112058000094.

[8] Suzen, Y. B., and Huang, P. G., "Modeling of flow transition using an intermittency transport equation," *Journal of Fluids Engineering*, Vol. 122, No. 2, 2000, pp. 273–284. doi:10.1115/1. 483255.

[9] Cho, J. R., and Chung, M. K., "A K-ϵ-γ equation turbulence model," *Journal of Fluid Mechanics*, Vol. 237, 1992, p. 301. doi:10.1017/S0022112092003422.

[10] Menter, F. R., Langtry, R. B., Likki, S. R., Suzen, Y. B., Huang, P. G., and Völker, S., "A correlation-based transition model using local variables—Part I: model formulation," *Journal of Turbomachinery*, Vol. 128, No. July 2006, 2006, p. 413. doi:10.1115/1.2184352.

[11] Langtry, R. B., Menter, F. R., Likki, S. R., Suzen, Y. B., Huang, P. G., and Völker, S., "A Correlation-Based Transition Model Using Local Variables—Part II: Test Cases and Industrial Applications," *Journal of Turbomachinery*, Vol. 128, No. 3, 2006, p. 423. doi:10.1115/1.2184353.

[12] Krause, M., Behr, M., and Ballmann, J., "Modeling of Transition Effects in Hypersonic Intake Flows Using a Correlation-Based Intermittency Model," *15th AIAA International Space Planes and Hypersonic Systems and Technologies Conference*, American Institute of Aeronautics and Astronautics, Reston, Virigina, 2008, pp. 1–12. doi:10.2514/6.2008-2598.

[13] Krause, M., "Numerical analysis of transition effects for SCRamjet intake flows," Ph.D. thesis, RWTH Aachen, 2010.

[14] Grabe, C., and Krumbein, A., "Prediction of Crossflow Transition," *52nd Aerospace Sciences Meeting*, 2014, pp. 1–14.

[15] Choi, C.-B., and Yang, K.-S., "Three-dimensional instability in flow past a rectangular cylinder ranging from a normal flat plate to a square cylinder," *Physics of Fluids*, Vol. 26, No. 6, 2014, p. 061702. doi:10.1063/1.4883176.

[16] Van den Eynde, J., Steelant, J., and Passaro, A., "Intermittency-based Transition Model with Local Empirical Correlations," *21st AIAA International Space Planes and Hypersonics Technologies Conference*, 2017, pp. 1–16.

[17] Blair, M. F., "Boundary-Layer Transition in Accelerating Flows With Intense Freestream Turbulence:

Part 1 -Disturbances Upstream of Transition Onset," *Journal of Fluids Engineering*, Vol. 114, No. 3, 1992, p. 313. doi:10.1115/1.2910032.

[18] Narasimha, R., "The laminar-turbulent transition zone in the boundray layer," *Progress in Aerospace Sciences*, Vol. 22, 1985, pp. 22–80. doi:10.1016/j.aqpro.2013.07.003.

[19] White, F. M., *Viscous fluid flow*, 2nd ed., McGraw-Hill, 1991.

[20] Langtry, R. B., and Menter, F. R., "Correlation-based transition modeling for unstructured parallelized computational fluid dynamics codes," *AIAA Journal*, Vol. 47, No. 12, 2009, pp. 2894–2906. doi:10.2514/1.42362.

[21] Abu-Ghannam, B. J., and Shaw, R., "Natural transition of boundary layers—the effects of turbulence, pressure gradient, and flow history," *Journal of Mechanical Engineering Science*, Vol. 22, No. 5, 1980, pp. 213–228. doi:10.1243/JMES_JOUR_1980_022_043_02.

[22] Mayle, R. E., "The Role of Laminar-Turbulent Transition in Gas Turbine Engines," *Journal of Turbomachinery*, Vol. 113, 1991, pp. 509–536.

[23] Steelant, J., and Dick, E., "A multigrid method for the compressible Navier—Stokes equations coupled to the k—ϵ turbulence equations," *International Journal of Numerical Methods for Heat & Fluid Flow*, Vol. 4, No. 2, 1994, pp. 99–113. doi:10.1108/EUM0000000004033.

[24] Dick, E., and Steelant, J., "Coupled solution of the steady compressible Navier-Stokes equations and the k$-\epsilon$ turbulence equations with a multigrid method," *Applied Numerical Mathematics*, Vol. 23, No. 1, 1997, pp. 49–61. doi:10.1016/S0168-9274(96)00061-X.

[25] Merci, B., Steelant, J., Vierendeels, J., Riemslagh, K., and Dick, E., "Computational Treatment of Source Terms in Two-Equation Turbulence Models," *AIAA Journal*, Vol. 38, No. 11, 2000, pp. 2085–2093. doi:10.2514/2.870.

[26] Menter, F. R., "Zonal Two Equation k-w Turbulence Models for Aerodynamic Flows," *24th Fluid Dynamics Conference*, 1993.

[27] Roach, P. E., and Brierley, D. H., "The influence of a turbulent free stream on zero pressure gradient transitional boundary layer development. Part 1: testcases T3A and T3B," *Numerical Simulation of Unsteady Flows and Transition to Turbulence*, Cambridge University Press, 1990, pp. 348–354.

[28] Sandham, N. D., Schülein, E., Wagner, A., Willems, S., and Steelant, J., "Transitional shock-wave/boundary-layer interactions in hypersonic flow," *Journal of Fluid Mechanics*, Vol. 752, 2014, pp. 349–382. doi:10.1017/jfm.2014.333.

[29] Schülein, E., "Effects of Laminar-Turbulent Transition on the Shock-Wave/Boundary-Layer Interaction," *AIAA Paper*, , No. June, 2014, pp. 1–23.

[30] Willems, S., Gülhan, A., and Steelant, J., "Experiments on the effect of laminar–turbulent transition on the SWBLI in H2K at Mach 6," *Experiments in Fluids*, Vol. 56, No. 3, 2015, p. 49. doi:10.1007/s00348-015-1904-z.

[31] Biagioni, L., and D'Agostino, L., "Measurement of energy spectra in weakly compressible turbulence," *30th Fluid Dynamics Conference, AIAA Paper 99-3516*, 1999.

[32] Passaro, A., "Hypersonic Aerothermodynamics Studies on Compression Corners," Ph.D. thesis, Università degli Studi di Pisa, Centrospazio, Pisa, Italy, 2003.

[33] Langtry, R. B., "A Correlation-Based Transition Model Using Local Variables for Unstructured CFD codes," Ph.D. thesis, University of Stuttgart, 2006.

[34] Sinha, K., Mahesh, K., and Candler, G. V., "Modeling the Effect of Shock Unsteadiness in Shock/Turbulent Boundary-Layer Interactions," *AIAA Journal*, Vol. 43, No. 3, 2005, pp. 586–594. doi:10.2514/1.8611.

[35] Jocksch, A., and Kleiser, L., "Growth of turbulent spots in high-speed boundary layers on a flat plate," *International Journal of Heat and Fluid Flow*, Vol. 29, No. 6, 2008, pp. 1543–1557. doi: 10.1016/j.ijheatfluidflow.2008.08.008.

[36] Jocksch, A., "Direct Numerical Simulation of Turbulent Spots in High-Speed Boundary Layers," Ph.D. thesis, Technische Universität Dresden, 2009. doi:10.1016/S0045-7930(01)00004-4.

[37] Redford, J. A., Sandham, N. D., and Roberts, G. T., "Numerical simulations of turbulent spots in supersonic boundary layers: Effects of Mach number and wall temperature," *Progress in Aerospace Sciences*, Vol. 52, 2012, pp. 67–79. doi:10.1016/j.paerosci.2011.08.002.

[38] Van den Eynde, J., and Steelant, J., "Compressibility and temperature effects on turbulent spot growth," *International Conference on High-Speed Vehicle Science Technology*, 2018.